2017 13th IEEE International Conference on Control & Automation (ICCA)
July 3-6, 2017. Ohrid, Macedonia

Hybrid Orientation Filter Aided Indoor Tracking for Pedestrians Using a Smartphone

Zhe Yang, Yun Pan, Ling Zhang

Abstract— **In this paper, we proposed a novel approach called Hybrid Orientation Filter which deploys a combination of the information filter and the complementary filter to achieve accurate heading estimation. Base on this approach, a Hybrid Orientation Filter aided pedestrian dead reckoning system with utilization of the visual gyroscope is proposed and implemented on a smartphone, offering real-time indoor tracking for pedestrians without map information or infrastructure. Experiment results show that the proposed dead reckoning system achieves typically sub-meter accuracy in position over 207 meters, and an average error of 2.55 degrees in heading over 1800 degrees.**

I. INTRODUCTION

Indoor tracking for pedestrians has been developing rapidly in recent years with growing demands for position based services. However, challenges still exist for desired accuracy and reliability is hard to achieve in Global Navigation Satellite System (GNSS) denied environments. Different methods can be utilized to solve this problem, among which, the Pedestrian Dead Reckoning (PDR) [1-6] is a widely used approach using dead reckoning to find the orientation and position of the pedestrian relative to an initial position, rather than using landmarks or infrastructure including Wi-Fi and Bluetooth. When PDR is performed on smartphones, step based approach with step length estimation is more commonly used since the instability of accelerometer has little influence on the whole system, compared with double integration of acceleration data. In a step-based PDR system, the position of the pedestrian (x_N, y_N) at the step N is presented in a defined coordinate system and is updated from a known starting position (x_0, y_0) as shown in (1), where L_i and θ_i denote the step length and the heading of the step N in the coordinate system. Different kinds of step length models in step-based approaches are developed and have good accuracy, while several sensors on a smartphone can be utilized to obtain the orientation of the device including the inertial measurement units (IMU) and cameras [1-12].

$$\begin{cases} x_N = x_0 + \sum_{i=1}^{N} L_i cos\theta_i \\ y_N = y_0 + \sum_{i=1}^{N} L_i sin\theta_i \end{cases} \quad (1)$$

Visual rotation estimation of moving cameras can be solved by several methods. Visual Odometry (VO) [7, 8] is the process of estimating the rotation and translation of an agent equipped with cameras. Using vanishing points like [8] produces bad results during sharp turns, and applications are limited when scenarios lack visibility of building boundaries. Since the absolute scale of VO is unknown with single camera, rotation angles between images are the only practical information, making the camera perform as "visual gyroscope" [9, 10]. Hartmann et al. in [9] used visual gyroscope to optimize all of the relative rotations for a group of frames, whose main drawback was slow processing rate and lack of feasibility of real-time application. Kamran et al. in [10] proposed an online gyroscope without considering 3D points nor optimization, and thus had less accuracy than offline methods. Besides, relative rotation between frames can also be derived from the simultaneous localization and mapping (SLAM) and structure from motion (SFM) based methods [11, 12], which are not efficient on mobile platforms due to time consuming tasks including mapping and optimization with bundle adjustment. Apart from the camera, the orientation of the smartphone as a rigid body can be completely characterized utilizing data extracted from the gyroscope and magnetometer [1-6]. The magnetometer has zero-drift over time since it produces absolute heading information from the geomagnetic field. However, it is rather susceptible to local magnetic field sources and inaccurate for sudden changes. The gyroscope, on the other hand, adjusts to sudden changes quickly, but as inertial sensor, it loses accuracy over a period of time owing to inherent non-zero sensor drift.

Data from the aforesaid sensors always lose accuracy when used alone. Various filters can be utilized to fuse sensor data and reduce measurement errors. Information filter [14] is a variation of the Kalman filter (KF) [13]. When the number of measurements increases, the conventional Kalman filter suffers from complicated computations. In the information filter, however, multiple measurements can be filtered simply by summing in the correction step, making the fusion fast and lightweight. The complementary filter (CF) [15], which can perform the function of a low-pass and a high-pass filter together, is another simpler alternative of the Kalman filter. Tian et al. in [2] proposed an Extended Kalman Filter (EKF) to determine the correct heading by fusing data from both magnetometer and gyroscope, which had to cope with complicated matrix computations. Kang et al. in [4] also fused these two sensors by multi-branch conditioning. In this work the average location and heading error over a 168.55 meter trajectory are 1.35 meters and 2.28 degrees, respectively. Fusion of the camera with IMU in [16] produced acceptable result for indoor tracking within 20 meters, which did not cover long-term tracking performance. Kundra et al. in [17] proposed an orientation estimator fusing the camera and IMU by using complementary filters and optical flow. The main drawback of this work is requiring wireless environments,

*Research supported by the Fundamental Research Funds for the Central Universities (No. 2017QNA5009) and the Zhejiang Provincial Natural Science Foundation of China (No. LY15F020008).

Z. Yang, Y. Pan and L. Zhang are with the College of Information Science and Electronic Engineering, Zhejiang University, Hangzhou 310027, China (e-mail: {yangzhevlsi, panyun, 21531012}@zju.edu.cn).

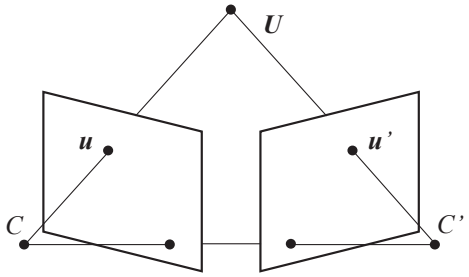

Figure 1. Epipolar geometry for two cameras.

which limits the scope of the application. Additional consideration such as map and physical constraints can help to improve the accuracy of the system using particle filter [6]. However, methods with map constraints require detailed knowledge of the environments, and particle filter becomes ineffectiveness when encountering scenes with few corridors.

In this paper, we propose a novel approach called Hybrid Orientation Filter (HOF) for orientation estimation, combining the information filter and complementary filter together. The HOF provides reliable long-term performances and rejects sensor drift together with environmental influence. Base on the HOF, we propose an HOF aided PDR system for pedestrian indoor tracking with no map information nor infrastructure (Wi-Fi, NFC, etc.) required in the buildings. The entire system is implemented in a real-time application on a ready-to-use smartphone device, with all data recorded and calculated by the smartphone only, making the system practical and convenient whenever encountering unknown indoor scenarios.

This paper is divided into five sections including this section. In Section 2, the visual gyroscope and the proposed Hybrid Orientation Filter are comprehensively described. The HOF aided PDR is presented in Section 3. Section 4 reports and discusses the experimental results. Finally, Section 5 concludes this paper.

II. METHODS

A. Visual Gyroscope

According to epipolar geometry in Fig. 1, a pair of images with point correspondences follow the epipolar constraint (2), where $\boldsymbol{E}$ is a 3×3 essential matrix consisting of a 3×3 rotation matrix $\boldsymbol{R}$ and a 3×1 translation vector $\boldsymbol{T}$ (~ means equality up to scale, and $[\boldsymbol{T}]_\times$ is the cross product matrix of $\boldsymbol{T}$) as shown in (3). The corresponding pixel points in the first and the second images are $\boldsymbol{u}$ and $\boldsymbol{u}'$. The camera's calibration matrix $\boldsymbol{K}$ in (4) can be obtained offline by experiments, where f is the focal length and x_{pp}, y_{pp} are principle points in images.

$$\boldsymbol{u}^T(\boldsymbol{K}^{-1})^T\boldsymbol{E}\boldsymbol{K}^{-1}\boldsymbol{u}' = 0 \tag{2}$$

$$\boldsymbol{E} \sim [\boldsymbol{T}]_\times \boldsymbol{R} \tag{3}$$

$$\boldsymbol{K} = \begin{bmatrix} f & 0 & x_{pp} \\ 0 & f & y_{pp} \\ 0 & 0 & 1 \end{bmatrix} \tag{4}$$

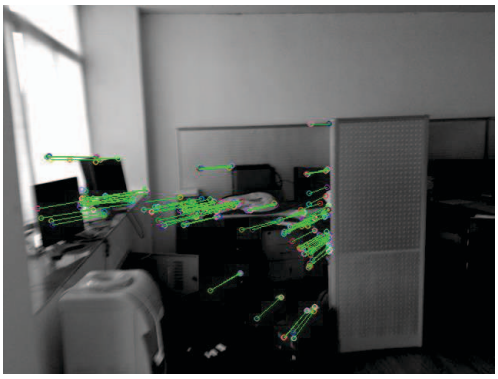

Figure 2. Finding ORB feature correspondences to estimate essential matrix.

To estimate essential matrix $\boldsymbol{E}$ efficiently, the five-point algorithm [18] is used here to solve the epipolar constraint and obtain rotation information. To recover rotation matrix $\boldsymbol{R}$, essential matrix $\boldsymbol{E}$ is decomposed using SVD decomposition as shown in (5) and (6). RANSAC (Random sample consensus) is applied to reject outliers in point correspondences, which was also covered in [18].

$$\boldsymbol{E} = \boldsymbol{U}\boldsymbol{\Lambda}\boldsymbol{V}^T \tag{5}$$

$$\boldsymbol{R} = \boldsymbol{U}\begin{bmatrix} 0 & -1 & 0 \\ 1 & 0 & 0 \\ 0 & 0 & 1 \end{bmatrix}\boldsymbol{V}^T \tag{6}$$

As to find point correspondences from two images, the visual gyroscope uses Oriented FAST and Rotated BRIEF (ORB) [19] as key point detector and feature descriptor for feature extraction and matching. Being binary descriptor, ORB is a good alternative to other vector based descriptors in computation cost and matching performance. Once the ORB features have been found in the current frame, the best k matching descriptors in the previous frame are retrieved using the K-Nearest Neighbor (KNN) clustering algorithm. Fig. 2 shows an example result for ORB features detection and matching between two frames, which can be further used to estimate rotation between frames.

B. Hybrid Orientation Filter

We proposed a Hybrid Orientation Filter which integrates the information filter and complementary filter in order to achieve more accurate and reliable orientation estimation, compared with sensors being used individually. Data from the gyroscope and visual gyroscope are first fused by the information filter in the HOF, which is summerized as the prediction phase in (7) and the correction phase in (8):

$$\begin{aligned} c &= m_{t-1/t-1}(m_{t-1/t-1} + q^{-1})^{-1} \\ m_{t/t-1} &= m_{t-1/t-1}(1-c)^2 + q^{-1}c^2 \\ v_{t/t-1} &= (1-c)v_{t-1/t-1} \end{aligned} \tag{7}$$

$$\begin{aligned} v_{t/t} &= v_{t/t-1} + r_{gyro}^{-1}h_{gyro,t} + r_{cam}^{-1}h_{cam,t} \\ m_{t/t} &= m_{t/t-1} + r_{gyro}^{-1} + r_{cam}^{-1} \\ h_{in,t} &= m_{t/t}^{-1}v_{t/t} \end{aligned} \tag{8}$$

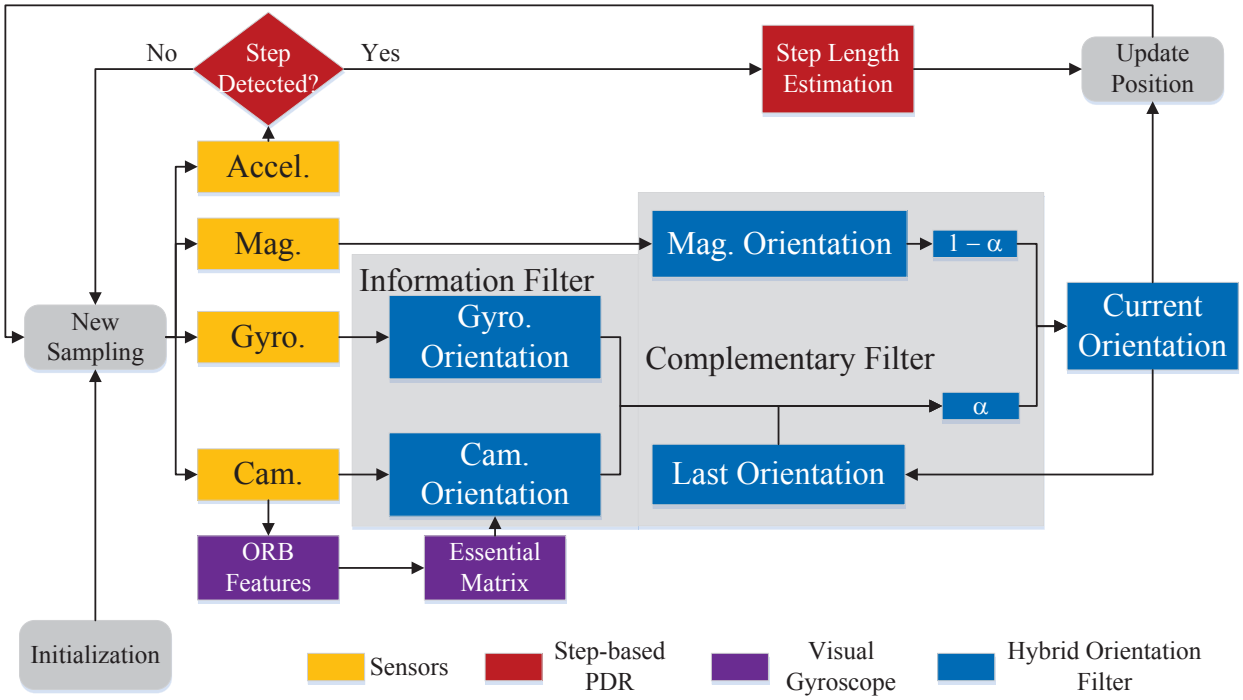

Figure 3. Overview of the Hybrid Orientation Filter aided PDR system.

where $h_{in,t}$ is the output of the information filter, with the heading data measured by the gyroscope and visual gyroscope at each time step t denoted by $h_{gyro,t}$ and $h_{cam,t}$, respectively. In order to simplify the computation expression, an intermediate variable is utilized here represented by c. The information matrix and vector of the information filter is presented by m and v, where t/t and t/t-1 indicate the state of correction and prediction. The inverse process noise covariance q^{-1}, together with the inverse measurement noise covariance from the gyroscope and visual gyroscope, denoted by r^{-1}_{gyro} and r^{-1}_{cam}, can be cached to reduce computation consumption. Due to motion blur and illumination variance, sometimes the gyroscope is the only trusted source of heading information since the visual gyroscope fails to estimate the rotation correctly. In detail, if the difference between angles from the gyroscope and visual gyroscope is more than a given threshold, the correction phase in (8) will not take data from the visual gyroscope into consideration, i.e. r^{-1}_{cam} and $r^{-1}_{cam}h_{cam,t}$ will not be added. The threshold in this paper is set to 6 degrees.

Data from the magnetometer and the output of the information filter will be then sent to the complementary filter:

$$h_{HOF,t} = \alpha(h_{HOF,t-1} + h_{in,t}) + (1-\alpha)h_{mag,t} \tag{9}$$

where $h_{HOF,t\text{-}1}$ and $h_{HOF,t}$ denotes the previous and current heading data filtered by the complementary filter. The low frequencies of drift from the heading data $h_{in,t}$ calculated by the information filter are necessary to be rejected. Meanwhile, for the orientation data $h_{mag,t}$ collected by the magnetometer, higher frequencies caused by local magnetic disturbance must be filtered. It is required to determine the proper ratio of each input signal using a constant α which determines cut-off frequency. The constant α in is set to 0.97 in this paper.

III. HOF Aided PDR System

The proposed HOF can be easily implemented into practical tracking applications. A step-based PDR system embedded with HOF is proposed in this section as shown in Fig. 3, where the blue parts denote the implementation of the HOF. The pedestrian is tracked while the phone is held in front of the body as shown in Fig. 4(a), which is a reasonable position and can be found commonly in [2-6]. The methods for step detection and step length estimation in [6] are used here since they achieved much better performances than previous work [2-5] on accuracy and robustness.

The step detection task is to find peaks of user's acceleration in vertical direction. The valid steps are achieved when the magnitude of peaks in vertical acceleration is greater than a given threshold. Fig. 4(b) shows the default coordinate system of accelerometer on the smartphone. When the smartphone is held horizontally, the vertical acceleration can be calculated under (10) where $grav_x$, $grav_z$, acc_x, acc_z represent the gravitational acceleration along x and z axis, and user's acceleration along x and z axis, respectively. Likewise, when we hold the smartphone vertically, $grav_x$ and acc_x should be changed to $grav_y$ and acc_y in (10), which represents the gravitational acceleration along y axis, and user acceleration along y axis, respectively.

$$\begin{aligned} \varphi &= atan\left(abs\left(grav_z / grav_x\right)\right) \\ acc_{vertical} &= acc_z * sin\varphi + acc_x * cos\varphi \end{aligned} \tag{10}$$

The step length is calculated by height and step frequency f as shown in (11), where k is a constant and equals 0.3139 for male and 0.2975 for female, while k_{ini} is set to 0.415 for male and 0.413 for female according to [6]. The step frequency equals to zero in the initial step. When the time interval

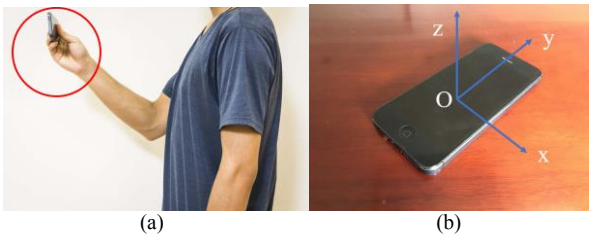

(a) (b)

Figure 4. (a) The smartphone's holding pose when being held. (b) Default smartphone's coordinate system.

between two valid steps is more than 2 seconds, the step frequency is set to zero as well.

$$L_s = \begin{cases} k * height * \sqrt{f} & , f > 0Hz \\ k_{ini} * height & , f = 0Hz \end{cases} \quad (11)$$

The orientation is estimated utilizing data from the HOF to achieve accurate heading data. Note that the gyroscope has a higher sample rate at 50Hz, however the visual gyroscope has a lower sample rate at 25Hz on account of large amounts of data and complex computations. These two data sampling tasks are delegated to two individual threads in the runtime application on the smartphone. The entire HOF aided PDR algorithm can be briefly summarized to the pseudo code presented in TABLE I.

TABLE I. PSEUDO CODE FOR HOF AIDED PDR

Initialization:
  Initialize m, v, r^{-1}_{gyro}, r^{-1}_{cam}, q^{-1}, h_{gyro}, h_{cam}, h_{mag}.
  Initialize current position P, and step length L_s.
  Start the IMU's thread and the camera's thread.

IMU's Thread: (at 50Hz)
  Get new acc, $grav$, $h_{mag,t}$ and Δh_{gyro} samples from the IMU.
  $h_{gyro,t} = h_{gyro,t-1} + \Delta h_{gyro}$
  Apply low-pass filter to acc. Get acc_{vertical} using acc and $grav$ by (10).
  Perform step detection.
  if step detected
    Get $h_{cam,t}$ from the camera's thread.
    Get current step frequency f. Calculate L_s using (11).
    if $| h_{gyro,t} - h_{cam,t} | < 6$ degrees
      $[m_{t/t}, v_{t/t}] = f_1(m_{t/t-1}, v_{t/t-1}, r^{-1}_{gyro}, r^{-1}_{cam}, h_{gyro,t}, h_{cam,t})$ using (8).
    else
      $[m_{t/t}, v_{t/t}] = f_1(m_{t/t-1}, v_{t/t-1}, r^{-1}_{gyro}, h_{gyro,t})$ using (8).
    end if
    $h_{HOF,t} = alpha(h_{HOF,t-1} + v_{t/t}/m_{t/t}) + (1 - alpha)h_{mag,t}$
    $P_t = P_{t-1} + L_s * cos(h_{HOF,t})$ and $L_s * sin(h_{HOF,t})$
    $[m_{t+1/t}, v_{t+1/t}] = f_2(m_{t/t}, v_{t/t}, q^{-1})$ using (7).
    Reset $h_{gyro,t}$ and $h_{cam,t}$.
  end if

Camera's Thread: (at 25Hz)
  Get current features $\{f_{i,curr}\}$. Match with previous feature$< f_{i,curr}, f_{i,prev} >$.
  if number of matched points > 5
    Estimate essential matrix $\boldsymbol{E}$ according to [18].
    Extract rotation matrix $\boldsymbol{R}$ using (5), (6).
    $h_{cam,t} = h_{cam,t-1} + arctan(-\boldsymbol{R}(3, 1), \boldsymbol{R}(3, 2)^2 + \boldsymbol{R}(2, 2)^2)$
  end if
  Swap $< f_{i,curr}, f_{i,prev} >$, clear $\{f_{i,curr}\}$.

IV. EXPERIMENTAL RESULTS

The proposed HOF aided PDR system was implemented in an application running on an iPhone 5. The average running time of the IMU's thread in TABLE I is 0.18 milliseconds, while the camera's thread has an average running time of 26.31 milliseconds. The experiment, which aims to track a user holding a smartphone in a realistic indoor environment, was deployed on the fifth floor of the Shengyi building in Zhejiang University in order to evaluate the accuracy of the HOF and HOF aided PDR system. The user walked along a predefined rectangular path and stopped at the starting point after 5 loops, with the total walking distance of approximately 207 meters. Different walking patterns like lines and corners were included, which made the experiment more convincing and corresponding to reality. As for evaluation of tracking performance, several checkpoints at known locations can be seen as blue circles in the ground truth provided in Fig. 5. The experiment was run on 5 participants including four men and a woman, and each participant repeated the same path three times. The average age of the participants is 23.8 years old, and the heights of the participants vary from 1.68 to 1.86 meters. The average results of the experiment are demonstrated as follows.

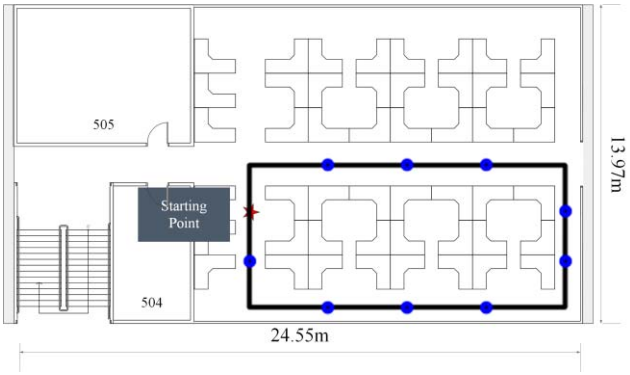

Figure 5. Ground truth with starting point and checkpoints (blue circles).

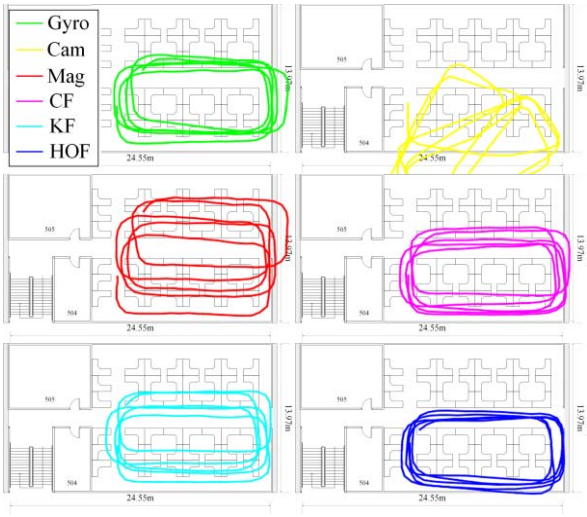

Figure 6. Trajectories with different orientation estimation.

Different kinds of orientation estimating method are adopted to determine orientation of each step, which are denoted by legends in the figures. The result of the proposed HOF aided PDR can be observed as the blue lines in the figures. The red lines, yellow lines and green lines represent

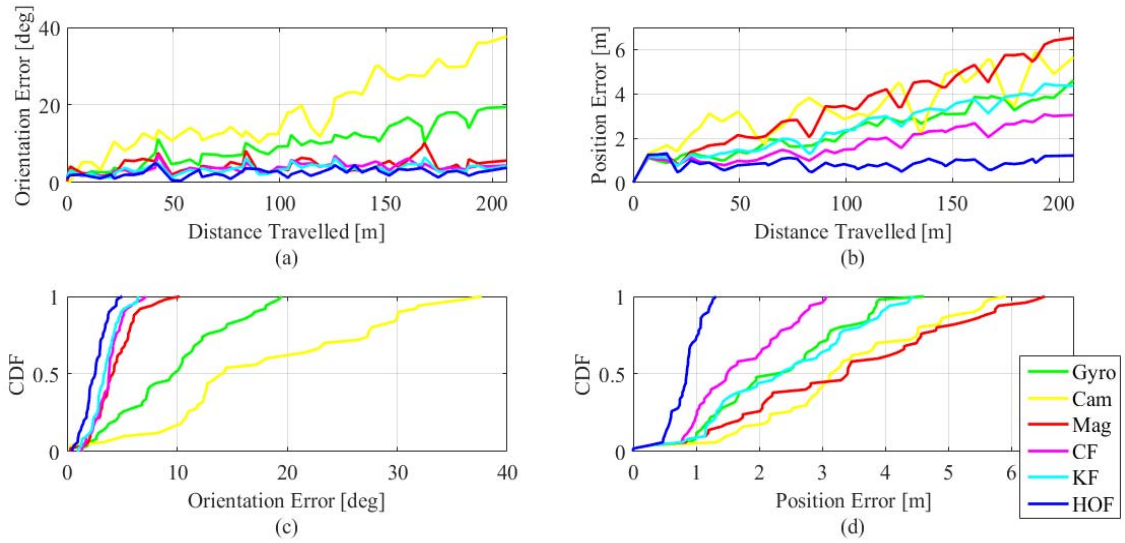

Figure 7. (a) Orientation error with respect to the ground-truth. (b) Position error with respect to the ground-truth. (c) Cumulative orientation error distribution with respect to the ground-truth. (d) Cumulative position error distribution with respect to the ground-truth.

dead reckoning using only the magnetometer, visual gyroscope and gyroscope, respectively. The magenta lines mean tracking trajectory combining the gyroscope, visual gyroscope and magnetometer using complementary filter as shown in (12) and (13):

$$h_t = \alpha(h_{t-1} + h_{x,t}) + (1-\alpha)h_{mag,t} \tag{12}$$

$$h_{x,t} = \frac{r_{cam}}{r_{gyro} + r_{cam}} h_{gyro,t} + \frac{r_{gyro}}{r_{gyro} + r_{cam}} h_{cam,t} \tag{13}$$

where r_{gyro} and r_{cam} denote noise covariance from the gyroscope and visual gyroscope. Fusing data from the gyroscope, visual gyroscope and magnetometer using the Kalman filter [13] in positioning is shown by the cyan lines, where the state vector of the Kalman filter is $[h, \Delta h]^T$ with h and Δh denoting the heading angle and angular velocity. The measurement vector of the Kalman filter is $[h_{mag,t}, h_{x,t}]^T$, with transition matrix $\boldsymbol{F} = [1, 1; 0, 1]$ and output matrix $\boldsymbol{H}$ equaling to identity matrix. Fig. 6 shows localization trajectories with different orientation estimation methods.

The accuracy of the PDR system is measured as $e(n) = \left\| P_n - \hat{P}_n \right\|$ at each checkpoint n, indicating the Euclidean distance between the estimated position $\hat{P}_n$ and the real position P_n. As for the orientation estimation, the absolute difference between the estimated orientation $\hat{h}_n$ and real orientation h_n is presented by $\xi(n) = \left| h_n - \hat{h}_n \right|$ at each checkpoint n. Fig. 7(a) and 7(b) show the orientation and position errors measured with respect to the reference data along the checkpoints. Fig. 7(c) and 7(d) present the cumulative distribution function (CDF) of the orientation and position errors. The average and standard deviation (STD) of the orientation and position errors for different methods can be found in TABLE II.

According to the tracking results, the gyroscope and visual gyroscope suffered from accumulation of sensor drift. In particular, motion blur and illumination variance had serious impact on the performance of the visual gyroscope, which made user out of orbit as the distance travelled increased. Though the magnetometer had a relatively smaller orientation drifting error, it always failed to cope with sudden changes; therefore, the tracking trajectory twisted throughout the route. Meanwhile, though fusing the gyroscope, visual gyroscope, and magnetometer by only the complementary filter or Kalman filter boosted accuracy in orientation estimation and positioning, the proposed Hybrid Orientation Filter achieved the best performance among the aforesaid approaches. The tracking trajectory estimated by HOF aided PDR system was the closest to the actual walking route in infrastructureless situation, with extremely small average position error. In detail, the average orientation error is 2.55 degrees with the total heading variance of 1800 degrees (i.e. 5 Loops). Besides, the average position error is 0.83 meters over a total walking distance of approximately 207 meters.

TABLE II. COMPARISON OF ORIENTATION AND POSITION ESTIMATION

	Approaches of orientation estimation					
	Gyro	***Cam***	***Mag***	***CF***	***KF***	***HOF***
Orientation error [deg] (mean±STD)	9.68±5.10	19.4±13.4	4.38±1.92	3.80±1.29	3.50±1.26	2.55±1.07
Position error [m] (mean±STD)	2.31±1.09	3.33±1.40	3.34±1.73	1.67±0.77	2.40±1.17	0.83±0.26

V. CONCLUSION

A novel orientation estimation approach called Hybrid Orientation Filter is presented in this paper. On the basis of this approach, this paper presents an HOF aided PDR system which is feasible to be implemented as real-time application on a ready-to-use smartphone due to its simple architecture and low computational complexity. When GNSS is unavailable, the proposed system achieves robust and reliable performances in realistic indoor tracking for pedestrians without exploiting any external infrastructure, which benefits the further integration of location based service. Future improvements can be achieved by extending the current 2-dimensional tracking to 3-dimensional applications and integrating the HOF aided PDR system with loop closure algorithms to improve the accuracy of indoor tracking.

REFERENCES

[1] K.-C. Lan and W.-Y. Shih, "On calibrating the sensor errors of a PDR-based indoor localization system," *Sensors*, vol. 13, no. 4, pp. 4781–4810, 2013.

[2] Z. Tian, Y. Zhang, M. Zhou, and Y. Liu, "Pedestrian dead reckoning for MARG navigation using a smartphone," *EURASIP Journal on Advances in Signal Processing*, vol. 2014, no. 1, p. 1, 2014.

[3] J. Qian, J. Ma, R. Ying, P. Liu, and L. Pei, "An improved indoor localization method using smartphone inertial sensors," in *Indoor Positioning and Indoor Navigation (IPIN), 2013 International Conference on*, 2013, pp. 1–7.

[4] W. Kang and Y. Han, "SmartPDR: Smartphone-based pedestrian dead reckoning for indoor localization," *IEEE Sensors Journal*, vol. 15, no. 5, pp. 2906–2916, May 2015.

[5] Q. Tian, Z. Salcic, Y. Pan, and others, "An enhanced pedestrian dead reckoning approach for pedestrian tracking using smartphones," in *Intelligent Sensors, Sensor Networks and Information Processing (ISSNIP), 2015 IEEE Tenth International Conference on*, 2015, pp. 1–6.

[6] Q. Tian, Z. Salcic, K. I.-K. Wang, and Y. Pan, "A hybrid indoor localization and navigation system with map matching for pedestrians using smartphones," *Sensors*, vol. 15, no. 12, pp. 30759–30783, 2015.

[7] D. Scaramuzza and F. Fraundorfer, "Visual Odometry [Tutorial]," *IEEE Robotics & Automation Magazine*, vol. 18, no. 4, pp. 80–92, Dec. 2011.

[8] L. Ruotsalainen, J. Bancroft, G. Lachapelle, H. Kuusniemi, and R. Chen, "Effect of camera characteristics on the accuracy of a visual gyroscope for indoor pedestrian navigation," in *Ubiquitous Positioning, Indoor Navigation, and Location Based Service (UPINLBS), 2012*, 2012, pp. 1–8.

[9] W. Hartmann, M. Havlena, and K. Schindler, "Visual gyroscope for accurate orientation estimation," in *2015 IEEE Winter Conference on Applications of Computer Vision*, 2015, pp. 286–293.

[10] D. Kamran, M. Karimian, A. Nazemipour, and M. T. Manzuri, "Online visual gyroscope for autonomous cars," in *Electrical Engineering (ICEE), 2016 24th Iranian Conference on*, 2016, pp. 113–118.

[11] A. J. Davison, I. D. Reid, N. D. Molton, and O. Stasse, "MonoSLAM: Real-time single camera SLAM," *IEEE Transactions on Pattern Analysis and Machine Intelligence*, vol. 29, no. 6, pp. 1052–1067, Jun. 2007.

[12] C. Wu, "Visualsfm: A visual structure from motion system, http://ccwu.me/vsfm, 2011," 2011.

[13] B. D. Anderson and J. B. Moore, *Optimal filtering*. Courier Corporation, 2012.

[14] X. Shen and P. K. Varshney, "Sensor selection based on generalized information gain for target tracking in large sensor networks," *IEEE Transactions on Signal Processing*, vol. 62, no. 2, pp. 363–375, 2014.

[15] M. B. Del Rosario, N. H. Lovell, and S. J. Redmond, "Quaternion-based complementary filter for attitude determination of a smartphone," *IEEE Sensors Journal*, vol. 16, no. 15, pp. 6008–6017, Aug. 2016.

[16] S. Tomažič and I. Škrjanc, "Fusion of visual odometry and inertial navigation system on a smartphone," *Computers in Industry*, vol. 74, pp. 119–134, Dec. 2015.

[17] L. Kundra, P. Ekler, and H. Charaf, "Wireless applications of mobile egomotion estimation with computer vision," in *European Wireless 2015; 21th European Wireless Conference; Proceedings of*, 2015, pp. 1–5.

[18] D. Nistér, "An efficient solution to the five-point relative pose problem," *Pattern Analysis and Machine Intelligence, IEEE Transactions on*, vol. 26, no. 6, pp. 756–770, 2004.

[19] E. Rublee, V. Rabaud, K. Konolige, and G. Bradski, "ORB: An efficient alternative to SIFT or SURF," in *2011 International conference on computer vision*, 2011, pp. 2564–2571.